Nuclear Magnetic Resonance study of molecular interaction of ionic liquids with aromatic compounds

Nuno M. C. G. Dias

Under Supervision of Fabián Vaca Chávez
Mestrado Integrado em Engenharia Física Tecnológica
Instituto Superior Técnico, Lisboa, Portugal

(Dated: November 25, 2013)

The liquid-liquid equilibria of ionic liquids (ILs) with chemicals and other solvents provide very important information to evaluate potential applications of IL such as chemical extraction and separation. In this thesis the effect on the molecular arrangements, dynamics and molecular interactions of binary mixtures of benzene and some of his fluorinated derivatives with the ionic liquid 1-ethyl-3-methyimidazolium bis((trifluoromethyl)sulfonyl)imide ([EMIM][NTf_2]) was studied. The fluorinated derivatives have different dipolar and/or quadrupolar moment which influence the solubility an the liquid-liquid equilibria, providing an excellent set of binary mixtures to carry out a systematic and exhaustive study. Using 1D and 2D nuclear magnetic ressonance (NMR) spectroscopy it was possible to obtain the arrangement of the cation of [EMIM][NTf_2] with the aromatic compounds as a function of the number of fluorine. Also, the results were explained based on the hydrogen bonds and the effect of the magnetic field created by the π electrons of the aromatic compounds. The information about the molecular dynamics was obtained from the NMR spin-lattice relaxation time. All protons on the IL move more freely in the mixtures (higher T_1) but a strong correlation with the quantity of fluorine in the aromatic compound was found.

Keywords: Ionic liquids, Fluorinated benzene, Aromatic compounds, Nuclear Magnetic Resonance, [EMIM][NTf_2], Binary mixtures

INTRODUCTION

Ionic liquids (ILs) are compounds composed solely by anions and cations (salts) which are in liquid state below 100 ^{o}C [1]. These compounds have had a growing attention in the last fifteen years by the scientific community and industry mainly due to their wide range of applications on engineering, biotechnology and material science. ILs can be used as solvents for catalytic reactions or chemical synthesis, as electrolytes in batteries [2, 3], capacitors [4], fuel cells [5], solar cells [6], CO_2 capture [7, 8], extraction of oil and tar from sand [9] and as chemical sensors [10]. These applications are due to their unique properties such as being liquid over a wide range of temperature, nonvolatile, nonflammable, relatively thermally and electrically stable and possessing an excellent dissolving power for a large number of organic and inorganic materials. The first IL was reported in the mid-19th century but it was at the beginning of the 20th century, one of the first room temperature IL was synthesized (ethylammonium nitrate, $C_2NH_8NO_3$) [1]. And it was only in the 70s and 80s that ILs were developed as electrolytes to be used in batteries [2, 3].

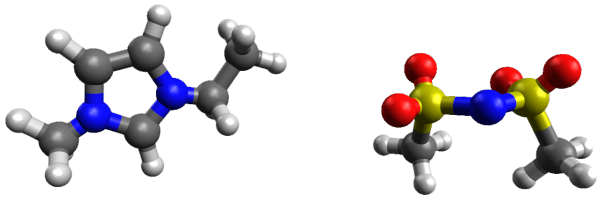

Figure 1: Structure of 1-ethyl-3-methylimidazolium bis(trifluoromethylsulfonyl)imide ($C_6H_{11}F_6N_3O_4S_2$, $T_m = 258$ K) [11].

Due to the unique physicochemical properties, ILs have been used in mixtures as co-solvent or as solvent. In this sense, theoretical and experimental studies of binary mixtures involving ILs are reported in the literature. Shiflett and Yokozeki [12] obtained all phase diagrams for the binary mixtures of 1-ethyl-3-methylimidazolium bis(trifluoromethylsulfonyl)imide ([EMIM][NTf_2])(Figure 1) with benzene and fluorinated benzenes (FBs) using only volume-mass measurements with a high-pressure experimental apparatus. Later, Shimizu *et al.* [13] performed molecular dynamics simulations (MDS) for the same mixtures using molecular dynamics algorithms, implemented in the DL_POLY program and they obtained the spatial distribution functions for the cation and the anion as well as the electrostatic charge distribution of the aromatic compounds.

Experimentally, NMR is widely used and a powerful technique that provides valuable and unique insights on the characterization of ILs from the structural and molecular dynamics point of view [8, 14]. The aim of this work is to obtain a detailed picture of the molecular interaction and local structure of solutions involving ILs. The binary mixtures composed by [EMIM][NTf_2], with several organic compounds with a wide range of dipolar and quadrupolar moments were studied. These organic compounds are a diverse group of benzene and FBs because they, when in liquid-liquid equilibria with [EMIM][NTf_2], exhibit unusual phase diagrams, which in some cases can go up to 80% mole fraction of aromatic compound dissolved in [EMIM][NTf_2] [12]. There are twelve fluorinated derivatives, with different dipolar and/or quadrupolar moment, so this set of binary mixtures is an excellent set to carry out a systematic and exhaustive study. The binary mixtures were studied using NMR spectroscopy and relaxometry.

All these results are useful to have a comprehension of the intra-molecular interactions of these mixtures and also to find new applications or design new technological processes.

THEORETICAL BACKGROUND

Ionic Liquids

We can ask ourselves why ILs are liquid at room temperature, and the commonly called salts are not. When salts are composed by mono atomic cations and anions, or by small molecules, salts pack nice and tightly in well organized structures at room temperature. Only at high temperatures, the thermal agitation of the atoms is enough to break them loose and so, the salt becomes liquid. But when the cation or the anion of the salt or both, have asymmetric structures a much smaller thermal energy to break the solid structure is needed, and so, the melting temperature is lower. As an example, magnesium sulfate ($MgSO_4$) has a melting temperature $T_m = 1397$ K while [BMIM][$CH_3CH(BF_3)CH_2CN$] melts at 189 K (Figure 2,) Nowadays, most of the cations

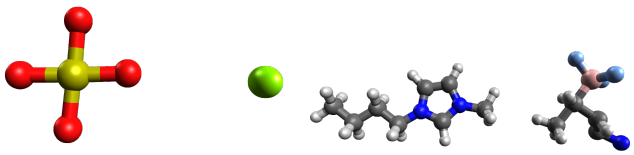

(a)Magnesium sulfate ($MgSO_4$, $T_m = 1397$ K)

(b) [BMIM][$CH_3CH(BF_3)CH_2CN$] ($C_{12}H_{21}BF_3N_3$, $T_m = 189$ K)

Figure 2: An example of a solid state salt at room temperature and an example of an IL [11].

used in the synthesis of ILs have an organic structure of low symmetry. When modifying the cation, is possible to change properties as the liquid range, the viscosity and the miscibility with other solvents. Among the wide range of possible ILs, the most studied are those which have as base the imidazolium cation [15]. Besides the thermophysical and thermodynamic properties as compressibilities, expansivities, heat capacities, densities, viscosities, speed of sound and pressure dependence of the heat capacity determined [16–19], several applications have been investigated. These kind of ILs have been used on extractive desulfurization of fuel oil [20](like [EMIM][DEP] or [BMIM][DBP]), as a renewable ferment [21] ([OMIM][PF_6]), to improve the CO_2 absorption performance, overcoming the disadvantages of high viscosity and poor gas-liquid mass-transfer of conventional methods [22], to modify inorganic nanoparticles to study their biomedical applications [23] and on the esterification of organic acid [24]. They can also be manipulated as an excellent solid phase extractant for lead on water [25] and used on the hydrolysis of cellulose due to their thermal stability and their ability to solubilize biomass [26].

Regarding the anion, $[NTf_2]^-$ based ILs are those which are most interesting regarding the water stability, high thermal stability, enhanced hydrophobicity, and relatively low viscosity [15, 27]. Several properties as compressibilities, expansivities, heat capacities, densities, viscosities, surface tensions and electrical condutivities have been determined [16, 18, 28] and several applications have been investigated. $[NTf_2]^-$ based ILs, such as [C_8mpyrr][NTf_2] or [C_8epip][NTf_2], have been used on pyrolysis [29], [C_1CnIm][NTf_2] was used for solvation of metallic nanoparticles [30], [BMPyr][NTf_2] as overlayer for estimating food quality [31], [C_2mim][NTf_2] on the processing and purification of nicotine [32]. Other $[NTf_2]^-$ based ILs were used in the removal of lead from water [25] and as a new type of solidlike layering [33].

Nuclear Magnetic Resonance

NMR is a physical phenomenon that occurs when magnetic nuclei are placed in an external magnetic field, this nuclei will absorb and re-emit electromagnetic radiation. It was firstly described by Isidor Raby in 1938 [34] and was latter on expanded for the use in liquids and solids by Felix Bloch and Edward Purcell in 1946. As a consequence, they were awarded with a Nobel Prize in physics in 1946 and 1952, respectively. NMR is widely used in medical diagnostics and chemical analysis and to determine molecular structures.

General overview

The magnetization will move around in an external magnetic field making a movement in a cone shape around the field as shown in Figure 3

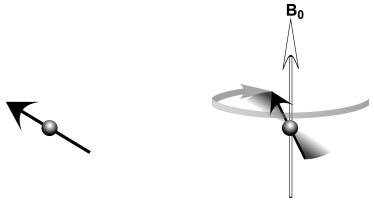

(a) (b)

Figure 3: Magnetization in the presence of an external magnetic field for $\gamma > 0$.

The precession frequency around the magnetic field is called Larmor frequency and is given by [35]

$$\nu_0 = \omega_0/2\pi = -\gamma\, B_0/2\pi \tag{1}$$

where B_0 is the external magnetic field, γ is the gyromagnetic ratio of a given particle. NMR can be used in all magnetic nuclei (non-null spin) when each nucleus has a precise resonance frequency depending on B_0 applied. In presence of B_0, a nucleus with a nuclear spin I has $2I+1$ energy levels with a spacing in energy between states given by [35],

$$\Delta E = \mu\, B_0/I = \gamma\, h\, B_0/2\pi \tag{2}$$

where $\mu = \gamma\, h\, I/2\pi$ is the nuclear magnetic moment. This energy difference between states will result in a small population difference when thermal equilibrium is reached, being the lowest energy state the most populated one.

Radio frequency pulses and relaxation

A radio frequency (RF) pulse generates a magnetic field with radio frequency oscillations, which, in the rotating frame, can be written as [35]

$$\mathbf{B}_{RF} = B_1\,\mathbf{e}_x. \tag{3}$$

If a RF is applied on resonance, the magnetization rotates around the x axis [35]. A RF pulse is a burst of radio waves with a given frequency and usually it has a very short period of time, usually on the order of microseconds (μs). If we apply the RF pulse using a coil in the x axis with a precise condition we can flip the magnetization to the y axis as is shown in Figure 4(a) and 4(b). This is called a 90^o pulse. The coil used to transmit the

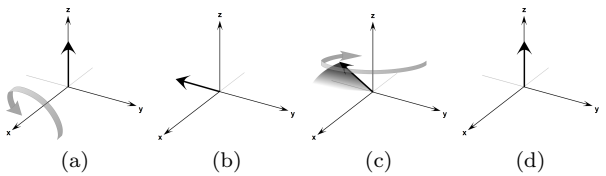

Figure 4: 90 degree pulse and the following relaxation of the magnetization.

RF pulse is also used as a receiver. The magnetization out of equilibrium induces a voltage on the coil, the NMR signal, that is called the free induction decay (FID).

Spin lattice relaxation time measurement

The spin-lattice or longitudinal relaxation time, T_1, is a NMR observable that depends on parameters as the temperature, viscosity, molecular arrangement, interactions and provides informations about the molecular motions [36]. Typical values of T_1 are from the milliseconds to tens of seconds. There is a well known pulse sequence in NMR to measure T_1 called inversion-recovery. This sequence consists on a 180^o pulse followed by a variable delay time τ and then by a 90^o pulse, as is sketched in Figure 5.

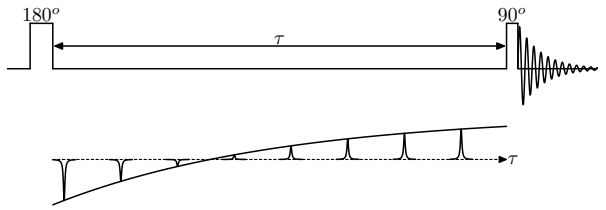

Figure 5: Inversion-recovery pulse sequence.

The 180^o pulse flips the magnetization (M_0) to the $-z$ axis and the FID is measured after a time $\tau = 0$ by applying a 90^o pulse. Performing this experiment for a set of different τ, the signal is then fitted using the equation $M_z(t) = M_0(1 - 2\exp(-t/T_1))$ to obtain T_1.

1D spectroscopy

After the FID is collected the NMR spectrum is obtained by performing the Fourier transform (FT). In cases where the signal to noise rato (SNR) is small, it is possible to overpass this drawback adding the spectra of repeated measurements. While the NMR signal adds linearly, the random noise will add slower and the signal to noise ratio (SNR) is given by,

$$SNR \propto \sqrt{ns}, \tag{4}$$

where ns is the number of scans. ^{13}C spectra can sometimes be difficult to analyze due to the overlapping peaks from different carbons. There is a technique used in NMR which is called decoupling. In this technique the sample is irradiated with a certain frequency in order to eliminate or partially eliminate the effect of coupling between spins. Decoupling is accomplished by applying a continuous low-power irradiation during the acquisition of the FID. Besides the simplification of the spectra, this effect can also help identify which pair of nuclei are involved in a J-coupling. One of the most used decoupling sequences is the Waltz-16. Figure 6 shows the sequence applied to obtain a proton decoupled ^{13}C spectrum. The pulse sequence consists on a repetition of a unit shown in Figure 6 [37]. The grey pulses mean that the phase is of $-x$ and

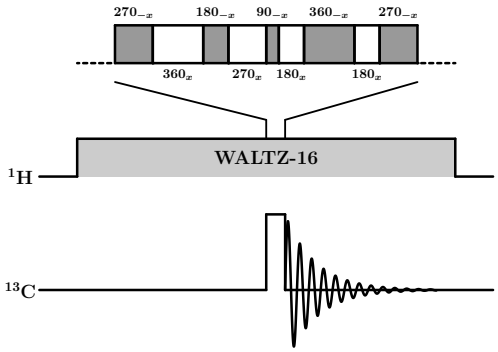

Figure 6: Schematic of the WALTZ-16 pulse sequence.

the white pulses of x. On the ^{13}C channel a 90^o hard pulse is applied while on the ^{1}H channel the WALTZ-16 composite pulse sequence is applied. In Figure 7 a ^{13}C and a ^{1}H decoupled ^{13}C spectra are shown, where it is observed the effect of the decoupling sequence is the collapse of several multiplets into singlets.

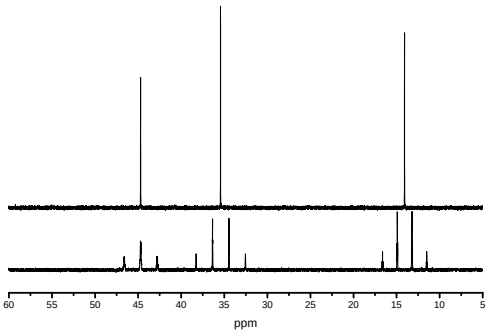

Figure 7: ^{13}C and ^{1}H decoupled ^{13}C spectra of [EMIM][NTf_2].

2D spectroscopy

Although some information can be extracted from 1D spectroscopy, it is limited to a single frequency scale. Two dimensions allow a better interpretation of some complex one dimensional spectra and gives information about the connectivity of nuclei on the sample. The second dimension comes from the recording of hundreds of 1D spectra, increasing a delay each time a measurement is done. The called nuclear Overhauser effect (NOE) is the base of the 2D nuclear Overhauser effect spectroscopy (NOESY) technique [36]. The NOE effect is a direct through space

interaction between two nucleus which are close in space (less than 5 Å). When a given nucleus is irradiated, all nucleus which are sufficiently close can feel an enhancement on their signal. This enhancement can go up to 2.99 in a ^{1}H ^{13}C pair or -3.93 in a ^{1}H ^{15}N pair. Basically, when we irradiate a given nucleus at his resonant frequency and we observe that the intensity of the signal of another nucleus is affected, we know that those two nuclei are close in space. The NOESY experiments pro-

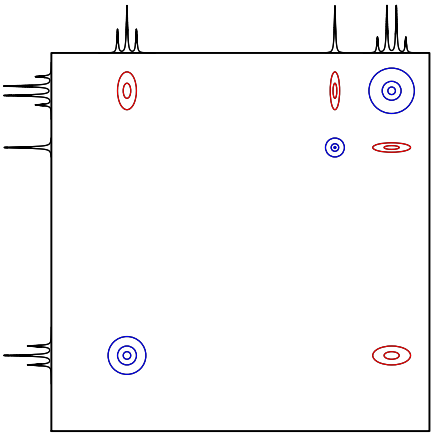

Figure 8: 2D spectrum of a NOESY experiment. Positive phased peaks are in blue and negative phased ones are in red.

duces a two-dimensional plot. On the diagonal there are positive phased peaks due too the auto-relaxation of the spins, the crossed peaks, on the contrary, usually have negative phased peaks [36]. In Figure 8 an example of a NOESY spectrum is shown, where the diagonal positive phased peaks are in blue and the negative phased peaks are in red. In this example the proton of the quadruplet interacts with the one of the triplet and with the one of the singlet, no interaction between the singlet and the triplet is observed.

Spin interactions

The interaction between spins with an external magnetic field was previously described and now we outline other spin interactions. The magnetic field felt by each nucleus is the sum over all magnetic fields created by all the spins in the sample, including the nuclear and electronic spins. The spin interactions that will be important to analyze the NMR results of this work are:

1. Chemical shift;
2. Indirect dipole-dipole coupling (J-coupling).

The chemical shift introduces a shift on the frequency of each spin. This shift for a given spin k is given by [36]:

$$\omega_k^0 = -\gamma_k B_0 (1 + \sigma_k^{iso}) \tag{5}$$

where σ^{iso} is the chemical shift in an isotropic liquid. This shift in ω_0 can be positive or negative, meaning that the nucleus will feel a stronger or weaker total magnetic field (less or more shielded). This shift is measured in parts per million (ppm) and is designated by δ, with $\delta = (f_{peak} - f_{ref})/f_{spec}$, being f_{ref} the frequency of the reference, and f_{spec} the spectrometer frequency and f_{peak} the frequency measured peak.

There are three important factors that influence the chemical shift: electron density, electronegativity and induced magnetic field effects.The first factor means that nuclear shielding is higher when the number surroundings electrons increases. Electronegativity is the tendency of a given atom or functional group to attract electrons. For example, in the case of a proton bounded to an oxygenated carbon (H−C−O), the proton will feel a deshielding effect (downfield shift). The electronegative oxygen pulls electrons, so the electrons will be a little displaced from the proton towards the carbon, so it will be more exposed to the external magnetic field. The third factor that influences the chemical shift can be explained with the classic example of the induced magnetic field effects is the benzene. The external magnetic field will make

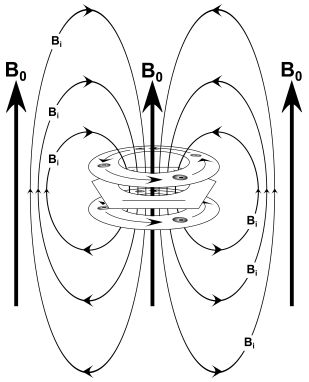

Figure 9: Induced magnetic field created by the π electrons of benzene on the presence of an external magnetic field.

the $\pi-$electrons of benzene to circulate (by Lenz's law) and thus create an induced magnetic field as depicted in Figure 9. This field will oppose the external magnetic field inside the ring, but will add to it outside. The benzene protons feel a strong induced field then they will be deshielded. The effect of the induced magnetic field might affect nucleus several Angstroms away, influencing their chemical shift.

The magnetic field created by each nuclear spin will affect the surrounding electron cloud, and this electron cloud will affect other nearby nuclei. This interaction is called indirect dipole-dipole or J-coupling because it is mediated through chemical bonds connecting the two nuclear spins. Observable coupling will usually not occur for nuclei separated by more than four bonds. For example, when a spin-1/2 is in the presence of an external magnetic field there will be a split in the energy as discussed in [36], with $\Delta E_0 = h\nu_0$ (Figure 10). In this situation there will be a single peak in the spectrum at ν_0 (Figure 10(b)). If we just consider a system with two J-coupled spin-1/2 nuclei, the surrounding electron cloud can increase or decrease the energy of the nuclear spin. If the spin of the electron cloud is parallel with the external magnetic field (ΔE_{02} in Figure 10), the energy difference between the nuclear 'up' state and down' state will be higher. If the spin of the electron cloud is anti-parallel with the magnetic field (ΔE_{01}) the energy difference will be smaller. Then, in the spectrum, in the presence of J-coupling the main peak at ν_0 will be split into two minor peaks with frequencies ν_{01} and ν_{02}, where $\Delta E_{01} = h\nu_{01}$

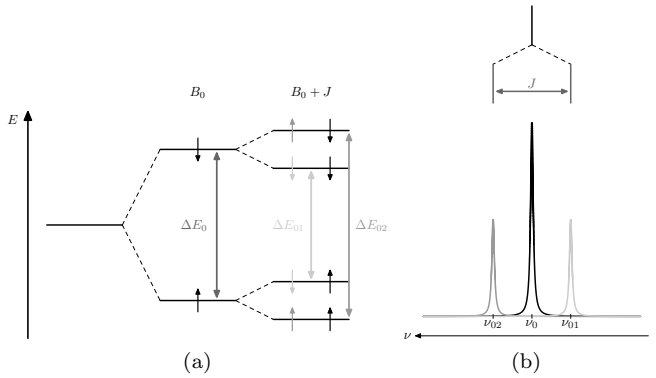

Figure 10: Energy splitting and frequency spectra in the presence of J-coupling.

and $\Delta E_{02} = h\nu_{02}$ (Figure 10(b)).

EXPERIMENTAL

Sample preparation

The aromatic compounds used were benzene, deuterated benzene, fluorobenzene, 1, 2-difluorobenzene, 1, 4-difluorobenzene, 1, 3, 5-trifluorobenzene, 1, 2, 4, 5-tetrafluorobenzene, pentafluorobenzene and hexafluorobenzene and the ionic liquid was 1-ethyl-3-methylimidazolium bis(trifluoromethylsulfonyl)imide. The samples were prepared by adding the aromatic compound to the IL and the concentration is expressed in molar fraction (mf) of aromatic compound, x, of benzene or its fluorinated derivatives. Almost all binary mixtures in study have a phase separation because they are not miscible in all proportions [12]. During the sample preparation, when the concentrations x_l was reached a phase separation was observed, where the subscript l correspond to the phase with lower concentration in benzene. In the same way, the subscript u is for the phase with higher concentration in benzene. Depending on the relative density of the components the lower phase corresponded to the phase rich in IL or in the aromatic compound. All mixtures were prepared at Instituto de Tecnologia Química e Biológica (ITQB) under a nitrogen atmosphere to avoid contamination from water, due to [EMIM][NTf_2] being very hygroscopic. The concentration is expressed in molar fraction (mf), x of benzene or its fluorinated derivatives. For almost every mixture four samples were prepared, $x = 0.10$, $x = 0.50$, $x = x_l$ and $x = x_u$. The only two exceptions are the $1, 3, 5$ FB because the immiscible region goes from the $x_l = 0.50 \pm 0.2$ to $x_u = 1.00 - 0.01$ [12], then only three concentrations were prepared. In the case of $1, 2$ FB which is miscible at all the concentrations, samples with $x = 0.10$, 0.30, 0.50, 0.60, 0.70, 0.80, 0.90, 0.96 and 0.99 were prepared. Figure 12 shows the molecular structure and the atom numbering of the IL and the aromatic compounds.

NMR measurements

The NMR measurements were performed at Laboratório de Cristais Líquidos at Instituto Superior Técnico (IST) at 23^o C. The reference compound used as a standard for calibrating the spectra was tetramethylsilane (TMS) ($Si(CH_3)_4$). TMS is a standard reference for ^{13}C and ^1H assigning the peaks to $\delta = 0$ ppm. A 5-mm NMR tube was filled with TMS and then, a capillar was inserted into the tube with the sample. The spectrometer used was a Bruker Avance II 300 equipped with a dual probe with ^1H and ^{13}C channel. The corresponding frequencies are 300.13 MHz and 75.47 MHz for ^1H and ^{13}C, respectively.

RESULTS

1D ^{1}H Spectroscopy

As the binary mixture of [EMIM][NTf_2] with $1, 2$ FB is miscible in all concentrations, it is a suitable system to show the effect of aromatic compounds on the spectrum of IL and *vice versa*. The spectra ^1H obtained for different concentrations are plotted in Figure 13(a). The atom numbering are defined in Figure 12.

Distinct behaviors are observed for the variation of the individual peaks. While all peaks move upfield (lower ppm) when the concentration of $1, 2$ FB is increased, H^2 moves upfield up to $x \cong 0.60$ and then is shifted downfield. H^6, H^7 and H^8 move downfield until around $x \cong 0.70$ and then the variation is approximately zero. H^4 and H^5 from the imidazolium ring and H^{10} and H^{11} from $1, 2$ FB move downfield across all the concentration range. To quantify the chemical shift variation of each ^1H we define $\Delta\delta = \delta_m - \delta_{pure}$, where δ_m is the measured value of the chemical shift for a given concentration and δ_{pure} is the value of the chemical shift in the pure [EMIM][NTf_2].

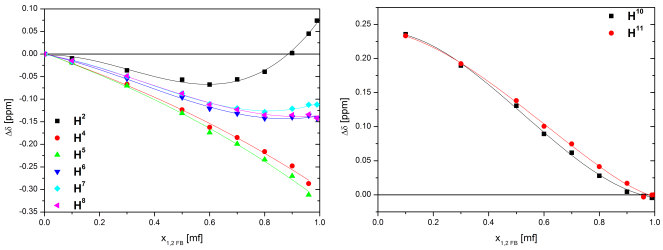

(a)^{1}H from [EMIM][NTf_2]. (b)^{1}H from $1, 2$ FB.

Figure 11: Chemical shift variation corresponding to the protons on the binary mixture of [EMIM][NTf_2] and $1, 2$ FB as a function of of the concentration of the aromatic compound. Solid lines are guide for the eyes.

Figure 11(a) shows the values of $\Delta\delta$ as a function of $x_{1,2\,\mathrm{FB}}$ for all protons of the cation and the variation of the chemical shift corresponding to the protons of $1, 2$ FB is presented in Figure 11(b). It can be observed that there are three different behaviors on the chemical shifts variation. One behavior is the one followed by H^2, the other is followed by H^6, H^7 and H^8 and the last one is the one of H^4 and H^5.

Spectra like the ones shown in Figure 13(a) were recorded for every binary mixture. The variation of the chemical shift for each proton of the IL was obtained for the different mixtures and the variation most representative proton, H^2, is presented in Figure 14. There is a trend that as the concentration of the aromatic compound increases, the chemical shift will be higher for

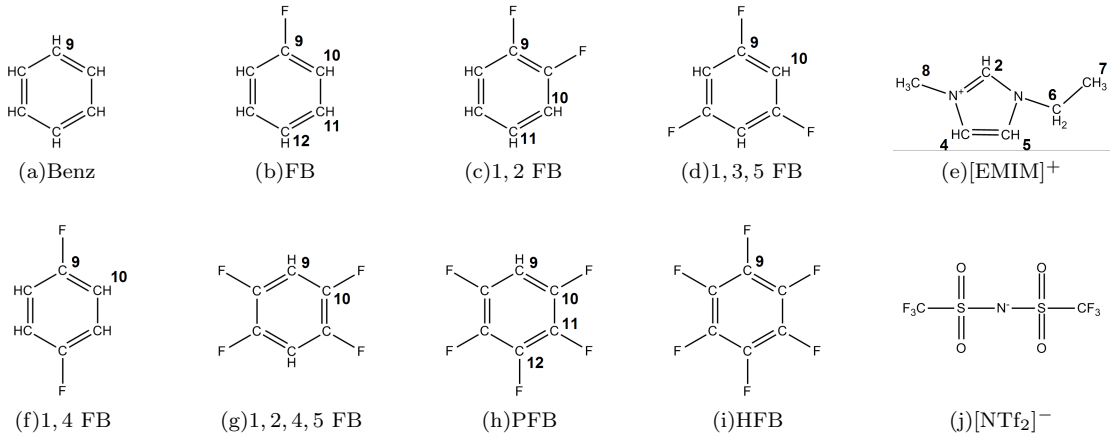

(a)Benz (b)FB (c)1, 2 FB (d)1, 3, 5 FB (e)$[EMIM]^+$

(f)1, 4 FB (g)1, 2, 4, 5 FB (h)PFB (i)HFB (j)$[NTf_2]^-$

Figure 12: Every compounds used on the binary mixtures with the assignment of each ^{1}H and ^{13}C.

those binary mixtures with more fluorines.

1D ^{13}C Spectroscopy

The proton decoupled carbon spectra of the binary mixture [EMIM][NTf_2] and 1, 2 FB for different concentrations are shown in Figure 13(b), where only the peaks from [EMIM][NTf_2] are displayed. The peaks corresponding to the 1, 2 FB are presented in 13(c). The peak of CF_3 is a quadruplet, but in Figure 13(b) just one of the peaks is plotted for simplicity to illustrate the chemical shift variation. The carbon of the CF_3, which is the only carbon on the anion, is the only one that is increasingly deshielded as the concentration of aromatic compound increases, C^2 and C^6 also show a deshielding but only after around $x \cong 0.70 - 0.80$. All the other carbons from [EMIM][NTf_2] feel an increasing shielding when the concentration of 1, 2 FB is increased. Now looking at the carbons of 1, 2 FB (Figure 13(c)) it is observed that the fluorinated carbon, C^9 (Figure 12(c)) has a negative chemical shift variation when the concentration in 1, 2 FB is decreased, and, on the contrary the protonated carbons, C^{10} and C^{10} (Figure 12(c)), present a positive chemical shift variation when the concentration of 1, 2 FB decreases. The variation of chemical shift for the different concentrations is summarized in Figure 15.

2D ^{1}H-^{1}H NOESY Spectroscopy

Using the pulse technique described previously, NOESY spectra were recorded for [EMIM][NTf_2] and the binary mixtures at $x = 0.50$. In Figure 16(a) the 2D spectra of the neat [EMIM][NTf_2] is shown. The diagonal positive phased peaks are in blue and the negative phased peaks are in red. It can be seen the interaction of H^7 with H^2, H^5 and H^6, the interaction of H^8 with H^2 and H^4 and finally H^6 with H^2 and with H^5. The spectra of 1, 4 FB is in Figure 16(b). The interactions between different protons are marked for clarity. The 1, 4 FB protons interact with H^6, H^7 and H^8.

Spin-lattice relaxation time measurements

The spin-lattice relaxation time was measured for all binary mixtures at 23^{o}C. The average T_1 of H^4 and H^5 was measured because in some cases the peaks were not resolved.

In Figure 17, T_1 as a function of the concentration of 1, 2 FB in the binary mixture with [EMIM][NTf_2] is shown. The T_1 value for all protons in the IL always increase when the concentration of the aromatic compound is increased (Figure 17(a)). There are three groups of T_1, the T_1 of H^2 is always close to the T_1 of H^4/H^5, the T_1 of H^6 with the one of H^8 and finally the T_1 of H^7 has values between these two last groups. The T_1 of the protons on the aromatic compound has the tendency to decrease when IL is added (Figure 17(b)), but the T_1 of H^{10}/H^{11} has a slight increase until around $x \cong= 0.96$.

Table I: T_1 values for the pure compounds [EMIM][NTf_2] and 1, 2 FB.

	H^2	H^4/H^5	H^6	H^7	H^8	H^{10}/H^{11}
T_1(ms)	1320.1	1357.5	627.7	929.6	548.0	4131.0

We can quantify the variation of T_1 and calculate the percentage variation $\Delta T_1/T_{1\text{pure}} = (T_{1\text{exp}} - T_{1\text{pure}})/T_{1\text{pure}}$, where $T_{1\text{exp}}$ is the experimental value determined and $T_{1\text{pure}}$ the value of the pure compound. The variation in percentage is shown in Figure 18.

We observe that the proton H^8 shows the higher variation on $\Delta T_1/T_{1\text{pure}}$. Also, the values of T_1 change up to 250% when 1, 2 FB is introduced on the sample.

DISCUSSION

2D ^{1}H-^{1}H NOESY

The NOESY data presented previously provides information about the spatial proximity between the protons of [EMIM][NTf_2] and the protons of the aromatic compound. The conclusions obtained from the spatial distribution functions determined by the MDS performed by Shimizu *et al.* [13] can be summarized as follows: the C^2 of the cation is close to the fluorines, and the oxygens of the anion will be close to the protons of the aromatic compounds. It can now be analyzed the case of 1, 4 FB (Figure 21), from MDS it is observed that the cation is near the fluorines or above the ring plane. From the information of the NOESY spectrum the H^6, H^7 and H^8

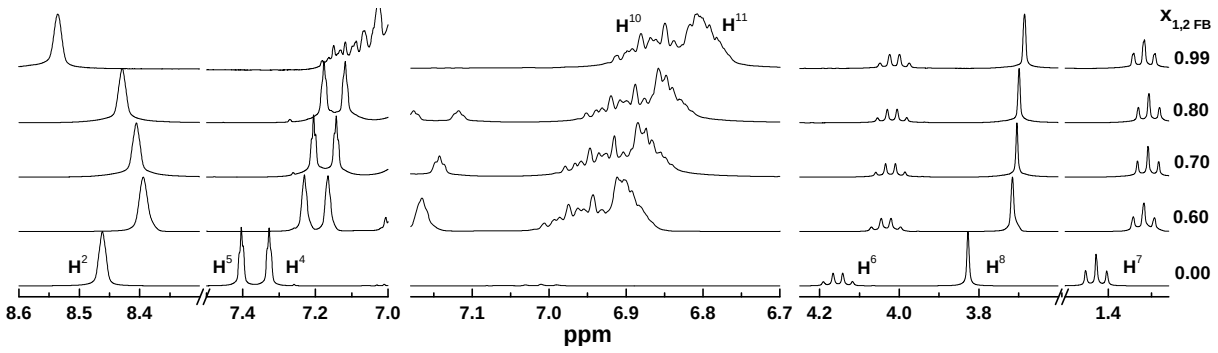

(a)^{1}H spectra

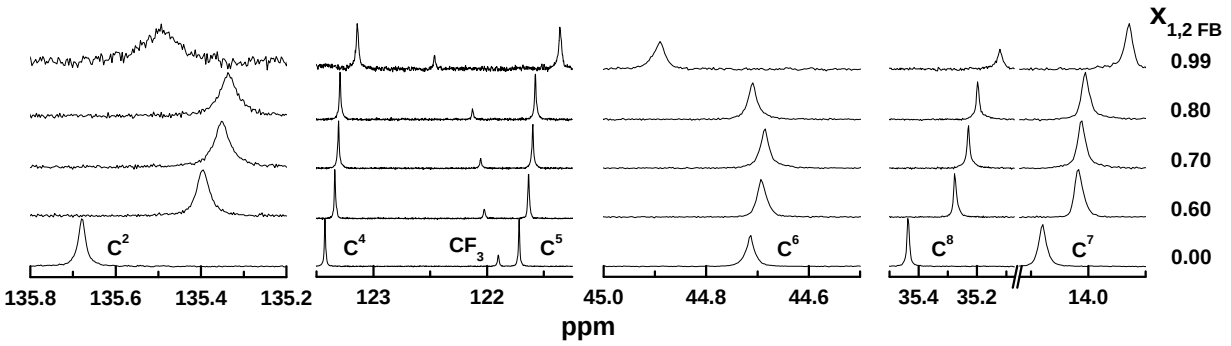

(b)^{1}H decoupled ^{13}C spectra

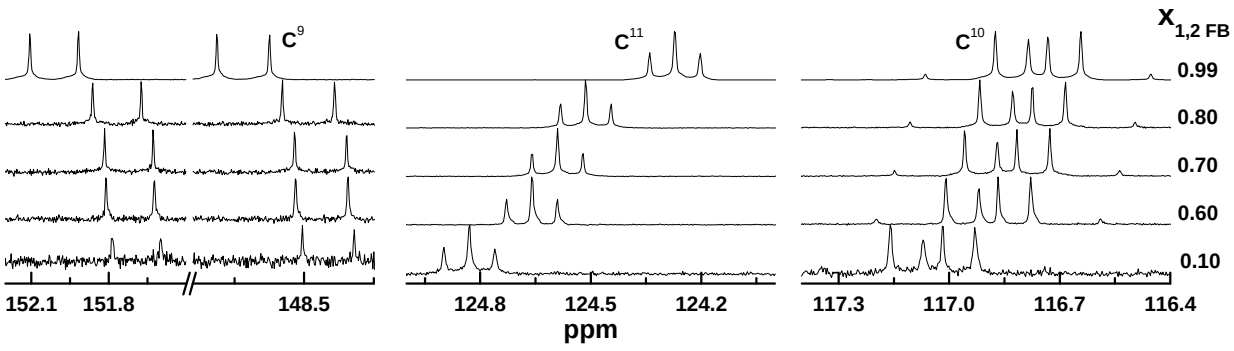

(c)^{1}H decoupled ^{13}C spectra

Figure 13: ^{1}H and ^{1}H decoupled ^{13}C spectra for the binary mixture of [EMIM][NTf$_2$] with 1, 2 FB. The series of spectra correspond to a) [EMIM][NTf$_2$], b) [EMIM][NTf$_2$] and c) 1, 2 FB.

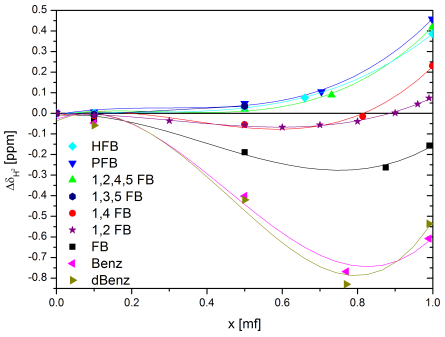

Figure 14: Chemical shift variation of H^2 for all binary mixtures as a function of concentration of the aromatic compound.

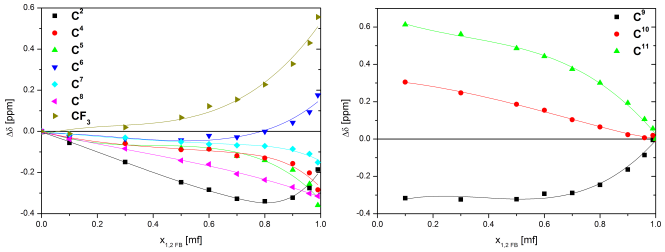

(a)^{13}C from [EMIM][NTf$_2$]. (b)^{13}C from 1, 2 FB.

Figure 15: Chemical shift plot for every carbon on the binary mixture of [EMIM][NTf$_2$] and 1, 2 FB.

interact with the protons of 1, 4 FB where the possible molecular orientations are shown in Figures 21(a), 21(b), 21(c) and 21(d).

The same analysis was done to all binary mixtures studied here. In the case of the mixture involving benzene, the cation is located above and below of the plane of the aromatic ring and the anion is around the protons of benzene (see Figure 19(a)). The increase of the number of fluorines in the aromatic compound, the cation, more precisely H^2, will be placed move closer to the fluorines, and the anion, more precisely origins, will stay near the protons of the aromatic ring. When six fluorines are on the aromatic compound, HFB, the cation will be all around the aromatic ring plane, close to the fluorines,

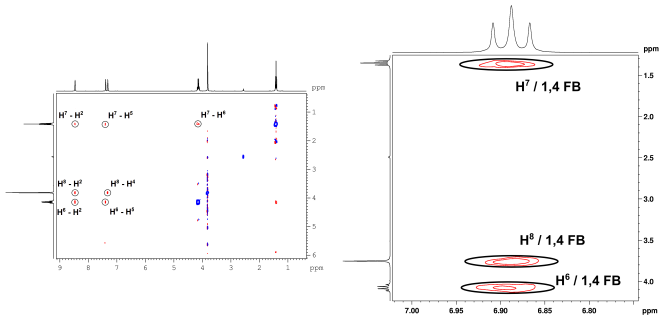

(a)[EMIM][NTf$_2$] (b)[EMIM][NTf$_2$] with 1, 4 FB

Figure 16: NOESY spectra of [EMIM][NTf$_2$] and of the mixture of [EMIM][NTf$_2$] with 1, 4 FB with $x = 0.50$. The positive phased peaks are drawn in blue and the negative phased peaks in red.

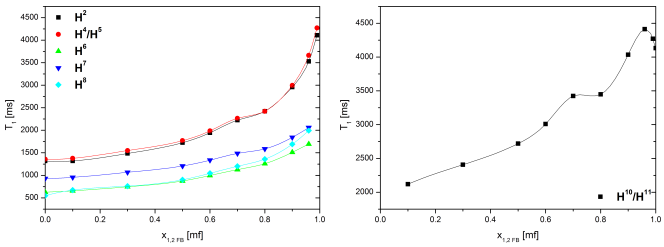

(a)^{1}H from [EMIM][NTf$_2$]. (b)^{1}H from 1, 2 FB.

Figure 17: T_1 for the binary mixture of 1, 2 FB with [EMIM][NTf$_2$].

and the anion will be on top and on the bottom of the aromatic ring plane (see Figure 19(b)).

1D Spectroscopy

In the pure IL, hydrogen bonds are formed between the cation and the anion. Hydrogen bonding is a special case of a dipole force. It is an attractive force in which hydrogen is bound to electronegative atoms such as nitrogen, oxygen or fluorine. H^2, H^4 and H^5 of the cation and the oxygens of the anion form hydrogen bonds in the pure [EMIM][NTf$_2$]. When an hydrogen bond is formed, the electron of the hydrogen will be pulled by the electronegative atom, leading to a deshielding of the proton of the hydrogen, resulting a positive chemical shift variation. When a hydrogen bond is weakened or broken, the opposite behavior will occur, and so the proton will be more shielded, what will lead to a negative chemical shift variation. In the case of the binary mixtures there are two competing processes influencing the chemical shift of the protons and carbons of the compounds: Hydrogen bonding and the ring current of the benzene and his fluorinated derivatives described before (Figure 9). If the protons are above or bellow the plane of the aromatic ring they will feel a smaller total magnetic field and so will be shielded, what will lead to a negative chemical shift variation. When the cation is around the aromatic ring, the protons will feel a higher total magnetic field and so will be deshielded what will result in a positive chemical shift variation.

As the sensitivity of ^{13}C is weaker than the one of ^{1}H, the chemical shift for most of the mixtures where $x \approx 0.99$, could not be determined and so the analysis for ^{13}C is limited. Nevertheless, the chemical shift variation

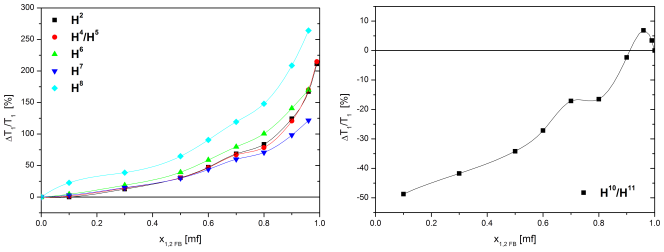

(a)^{1}H from [EMIM][NTf$_2$]. (b)^{1}H from 1, 2 FB.

Figure 18: Normalized T_1 variations for the binary mixture of [EMIM][NTf$_2$] and 1, 2 FB. The variation and the normalization is concerning the T_1 of the pure compounds.

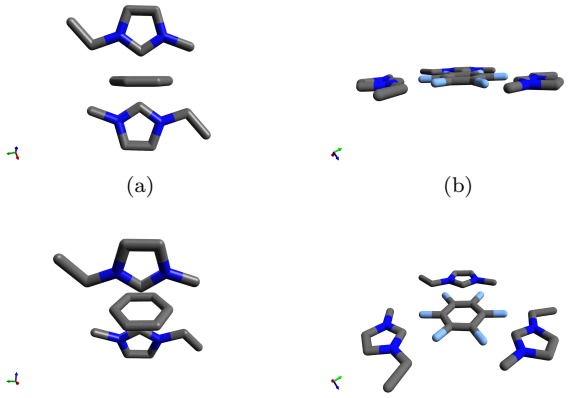

Figure 19: One of the possible arrangements of [EMIM]$^+$ regarding Benz and HFB. Images from the top row are in a side view and the images on the bottom row are in a tilted point of view.

of C^2 corroborates the conclusions obtained for H^2 showing that when the aromatic compound is introduced, the hydrogen bond will be weakened leading to a negative chemical shift variation, but around $x = 0.80$ the effect of the induced magnetic field begins to be more important and so C^2 moves to higher chemical shift variations (Figure 15(a)).

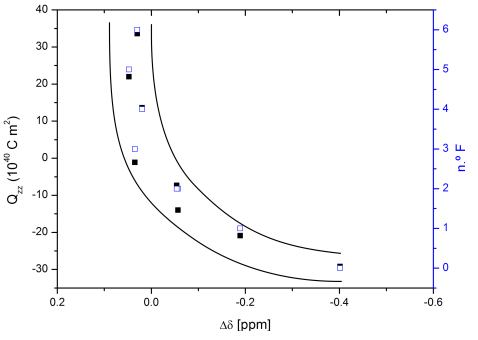

Figure 20: Relation between Q_{zz}, $\Delta\delta$ and the number of fluorines on benzene.

It is known that the quadrupolar and dipolar moment of benzene and his fluorinated derivatives play a key role on the solubility of [EMIM][NTf$_2$] [13]. In consequence, we can try to correlate this properties with our results. Q_{zz} increases when more fluorines are present in the aromatic compound. In Figure 20 the number of fluorines is related with Q_{zz} and with the chemical shift of H^2 at $x = 0.50$ for all binary mixtures. Q_{zz} is closely related with the number of fluorines on the aromatic compound

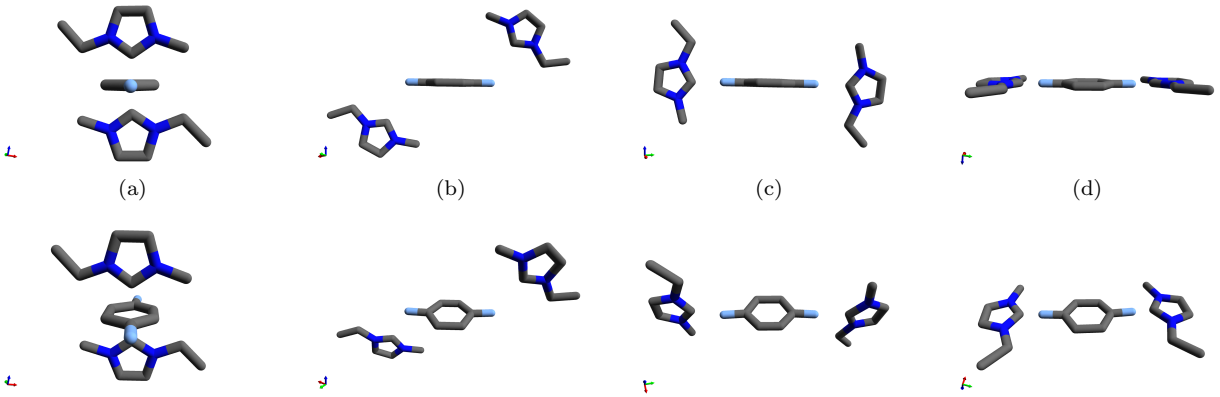

Figure 21: Arrangement of $[EMIM]^+$ regarding 1, 4 FB. Images from the top row are in a side view and the images on the bottom row are in a tilted point of view.

and both are related with $\Delta\delta$. This effect can be explained based on the discussion about the arrangement of the molecules presented previously.

In the mixture of benzene with [EMIM][NTf_2] the arrangement of H^2 is above and below the aromatic ring plane, feeling a smaller total magnetic field (more shielded), then shifted to lower chemical shift in comparison with the neat IL. As the number of fluorines is increased, the position of H^2 will change progressively to the plane of the aromatic ring, close to the fluorines. So, it will feel a bigger total magnetic field due to the field created by the ring current, what will lead to a decrease on the chemical shift. For three fluorines or more on the aromatic ring, the position of H^2 does not change much, and so $\Delta\delta$ is approximately constant for 1, 3, 5 FB, 1, 2, 4, 5 FB, PFB and HFB.

Spin-lattice relaxation time

To describe the spin-lattice relaxation time in isotropic liquids Bloembergen, Purcell and Pound considered a simple exponential form for the autocorrelation function given by [35]

$$G(t) \propto e^{-t/\tau_c} \tag{6}$$

where τ_c is the correlation time.

In the case of homonuclear dipolar interactions, the relaxation time is related with the spectral densities, $\mathbb{J}$, as [35]:

$$\frac{1}{T_1} = A\left[\mathbb{J}_1(\omega_0) + \mathbb{J}_2(2\,\omega_0)\right], \tag{7}$$

where $\mathbb{J}(\omega_0)$ is the FT of the autocorrelation function, $A \propto 1/r^6$ and r is the internuclear distance.

In the case of isotropic motions, from Eq. 6, we obtain:

$$\frac{1}{T_1} = A\left[\frac{\tau_c}{1+(\omega_0\tau_c)^2} + \frac{4\tau_c}{1+(2\omega_0\tau_c)^2}\right]. \tag{8}$$

A plot of T_1 is presented in Figure 22, with $\omega_0 = 2\pi \times 300 \times 10^6 Hz = 2 \times 10^9$rad/sec, and assuming a value of $\tau_c = 10^{-10}$ sec. Two regions are highlighted in Figure 22 corresponding to the "fast motions" ($\omega_0\tau_c << 1$) and "slow motions" ($\omega_0\tau_c >> 1$) regimes. In the fast motions regime, $1/T_1 \propto \tau_c$, which implies that an increase in T_1 means a decrease in τ_c.

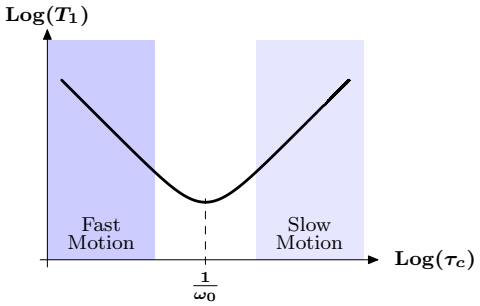

Figure 22: Spin lattice relaxation time vs the correlation time according to the BPP theory. The fast and slow motions regimes are highlighted.

For the results obtained in this work, we can assume that the motions of the IL and the aromatic compounds are in the fast motions regime. In Figure 18(a) it is observed that for all protons T_1 increases when the concentration of 1, 2 FB is increased. Assuming that the motions are in the fast motion regime, it can be concluded that when in mixture, all protons in the IL have a faster motion. The proton which possesses the highest increase, in percentage, is H^8 when the aromatic compound is added. If we look now to the $\Delta T_1/T_1$ of H^{10}/H^{11} (see Figure 18(b)) it is observed that T_1 decreases when the concentration of the IL is increased, except for concentrations higher than $x \sim 0.90$. This behavior will be object of further studies. Assuming that the fast motion condition is applicable to the aromatic molecule, the more [EMIM][NTf_2] we add to 1, 2 FB, the slower the motion will be.

CONCLUSIONS

In this work the molecular interaction and the local structure of the binary mixture of the ionic liquid [EMIM][NTf_2] with benzene and some of its fluorinated derivatives were studied. These binary mixtures were studied using 1D NMR spectroscopy, including ^{1}H, ^{13}C and as well as 2D spectroscopy (NOESY). The measurement of the proton spin-lattice relaxation times was also performed to study the molecular dynamics.

A strong correlation of the number of fluorines on the aromatic compound with the arrangement of the cation and the anion of the IL was found. In the pure IL the imidazilium ring protons form hydrogen bonds

with oxygens of the anion [13]. When [EMIM][NTf_2] is mixed with the aromatic compound the H^2 proton from $[EMIM]^+$ was found to be preferentially close to the fluorine on the aromatic compound and the oxygens of bis((trifluoromethyl)sulfonyl)imide ($[NTf_2]^-$) was found to be close to the protons of the aromatic ring. The H^2 showed to be more sensitive to the presence of the aromatic compounds, which was reflected on the chemical shift variation. The other two protons from the imidazolium ring present a similar behavior in the presence of the aromatic molecules. The 1D spectroscopy data showed that the effect of hydrogen bonds and ring currents are responsible of the chemical shift behavior due to the varied scenarios present in the binary mixtures. These two effects affect in different way the protons of the cation. A strong correlation was observed between the number of fluorines on the aromatic ring, the z component of the quadrupolar moment (Q_{zz}) of the aromatic compound and the chemical shift variation of the most acidic proton of the imidazolium ring (H^2). It was found that the chemical shift variation of the H^2 decreases and z component of the quadrupolar moment increases when the number of fluorines is higher. By using H^1-H^1 NOESY it was possible to obtain the molecular arrangement of the cation of [EMIM][NTf_2] respect to the aromatic compounds. The NOESY data provided a valuable information about the possible molecular arrangement for each binary mixtures studied, which were consistent with the molecular dynamic simulations performed by Shimizu *et al.* [13].

Finally, concerning the dynamics of the mixture, it was found that the spin lattice relaxation time corresponding to all protons on the cation increases when the concentration of aromatic molecules is higher. Assuming that the motions are in the "fast motions regime" it implies a decrease of the correlation time. Comparing the different protons, the protons of the methyl group closer to the imidazolium ring (H^8) shows the highest variation, in percentage. All protons of the aromatic compounds have a smaller T_1 when in mixture with [EMIM][NTf_2] probably a consequence of the molecular arrangement that slow down the molecular dynamics.

[1] P. Wasserscheid and T. Welton, *Ionic Liquids in Synthesis* (Wiley, 2008).

[2] H. L. Chum, V. R. Koch, L. L. Miller, and R. A. Osteryoung, J. Am. Chem. Soc. **97**, 3264 (1975).

[3] J. S. Wilkes, J. A. Levisky, R. A. Wilson, and C. Hussey, Inorganic Chemi **21**, 1263 (1982).

[4] A. Lewandowski and M. Galiński, Journal of Physics and Chemistry of Solids **65**, 281 (2004).

[5] R. F. de Souza, J. C. Padilha, R. S. Gonçalves, and J. Dupont, Electrochem. Commun. **5**, 728 (2003).

[6] E. Guillen, J. Idigoras, T. Berger, J. A. Anta, C. Fernandez-Lorenzo, R. Alcantara, J. Navas, and J. Martin-Calleja, Phys. Chem. Chem. Phys. **13**, 207 (2011).

[7] M. Ramdin, T. W. de Loos, and T. J. Vlugt, Ind. Eng. Chem. Res. **51**, 8149 (2012).

[8] M. Besnard, M. I. Cabaço, F. Vaca Chávez, N. Pinaud, P. J. Sebastião, J. A. P. Coutinho, J. Mascetti, and Y. Danten, J. Phys. Chem. A **116**, 4890 (2012).

[9] X. Li, W. Sun, G. Wu, L. He, H. Li, and H. Sui, Energ. Fuel. **25**, 5224 (2011).

[10] V. Singh, A. K. Nigam, A. Batra, M. Boopathi, B. Singh, and R. Vijayaraghavan, Intern. J. Electrochem. **2012**, 19 (2012).

[11] S. Zhang, X. Lu, Q. Zhou, X. Li, X. Zhang, and S. Li, *Ionic Liquids:: Physicochemical Properties* (Elsevier Science, 2009).

[12] M. B. Shiflett and A. Yokozeki, J. Chem. Eng. Data **53**, 2683 (2008).

[13] K. Shimizu, M. F. Costa Gomes, A. A. H. Padua, L. P. N. Rebelo, and J. N. Canongia Lopes, J. Phys. Chem. B **113**, 9894 (2009).

[14] H. Weingärtner, Curr. Opin. Colloid. In. Science **18**, 183 (2013).

[15] F. S. Oliveira, M. G. Freire, P. J. Carvalho, J. a. A. P. Coutinho, J. N. C. Lopes, L. P. N. Rebelo, and I. M. Marrucho, J. Chem. Eng. Data **55**, 4514 (2010).

[16] R. G. de Azevedo, J. Esperança, J. Szydlowski, Z. Visak, P. Pires, H. Guedes, and L. Rebelo, J. Chem. Thermodyn. **37**, 888 (2005).

[17] P. J. Carvalho, T. Regueira, L. M. N. B. F. Santos, J. Fernandez, and J. a. A. P. Coutinho, J. Chem. Eng. Data **55**, 645 (2010).

[18] J. M. S. S. Esperança, Z. P. Visak, N. V. Plechkova, K. R. Seddon, H. J. R. Guedes, and L. P. N. Rebelo, J. Chem. Eng. Data **51**, 2009 (2006).

[19] R. L. Gardas, M. G. Freire, P. J. Carvalho, I. M. Marrucho, I. M. A. Fonseca, A. G. M. Ferreira, and J. A. P. Coutinho, J. Chem. Eng. Data **52**, 80 (2007).

[20] Y. Nie, C.-X. Li, and Z.-H. Wang, Ind. Eng. Chem. Res. **46**, 5108 (2007).

[21] M. Freemantle, Chem. Eng. News Archive **79**, 57 (2001).

[22] M. Wang, L. Zhang, L. Gao, K. Pi, J. Zhang, and C. Zheng, Energ. Fuel. **27**, 461 (2013).

[23] A. Narita, K. Naka, and Y. Chujo, "Preparation of ionic liquid-modified inorganic nanoparticles and their biomedical application," in *Ionic Liquid Applications: Pharmaceuticals, Therapeutics, and Biotechnology* (ACS Symposium Series, 2010) Chap. 10, pp. 103–114.

[24] W.-M. Xiong, M.-Z. Zhu, L. Deng, Y. Fu, and Q.-X. Guo, Energ. Fuel. **23**, 2278 (2009).

[25] M. E. Mahmoud, Desalination **266**, 119 (2011).

[26] S. Bose, D. W. Armstrong, and J. W. Petrich, J. Phys. Chem. B **114**, 8221 (2010).

[27] Q.-S. Liu, P.-P. Li, U. Welz-Biermann, J. Chen, and X.-X. Liu, J. Chem. Thermodyn. **66**, 88 (2013).

[28] Q.-S. Liu, Z. Li, U. Welz-Biermann, C.-P. Li, and X.-X. Liu, J. Chem. Eng. Data **58**, 93 (2013).

[29] G. Chatel, R. Pflieger, E. Naffrechoux, S. I. Nikitenko, J. Suptil, C. Goux-Henry, N. Kardos, B. Andrioletti, and M. Draye, ACS Sustainable Chem. Eng. **1**, 137 (2013).

[30] A. Podgorsek, A. S. Pensado, C. C. Santini, M. F. Costa Gomes, and A. A. H. Pádua, J. Phys. Chem. C **117**, 3537 (2013).

[31] R. Toniolo, A. Pizzariello, N. Dossi, S. Lorenzon, O. Abollino, and G. Bontempelli, Anal. Chem. **85**, 7241 (2013).

[32] Z. P. Visak, S. L. Yague, J. N. C. Lopes, and L. P. N. Rebelo, J. Phys. Chem. B **111**, 7934 (2007).

[33] S. Bovio, A. Podestà, C. Lenardi, and P. Milani, J. Phys. Chem. B **113**, 6600 (2009).

[34] I. I. Rabi, J. R. Zacharias, S. Millman, and P. Kusch, Phys. Rev. **53**, 318 (1938).

[35] C. Slichter, *Principles of Magnetic Resonance*, Lecture Notes in Computer Science (Springer, 1990).

[36] M. Levitt, *Spin Dynamics: Basics of Nuclear Magnetic Resonance* (Wiley, 2008).

[37] N. Jacobsen, *NMR Spectroscopy Explained: Simplified Theory, Applications and Examples for Organic Chemistry and Structural Biology* (Wiley, 2007).